https://dx.doi.org/10.21577/0103-5053.20210049

J. Braz. Chem. Soc., Vol. 32, No. 8, 1519-1530, 2021

Article

Complexes with Furyl-Substituted 3-Hydroxychromone: Synthesis, Characterization and Fluorescence Studies

Mariana Leticia M. Camargo,[a] Fábio A. dos Santos,[b] Lucas Pizzuti,[a] Ulrich Abram[c] and Vânia Denise Schwade[*,a,d]

[a]*Laboratório de Síntese e Caracterização Molecular, Faculdade de Ciências Exatas e Tecnologia, Universidade Federal da Grande Dourados, 79804-970 Dourados-MS, Brazil*

[b]*Grupo de Pesquisa de Materiais Fotônicos e Energia Renovável, Faculdade de Ciências Exatas e Tecnologia, Universidade Federal da Grande Dourados, 79804-970 Dourados-MS, Brazil*

[c]*Institute of Chemistry and Biochemistry, Freie Universität Berlin, D-14195 Berlin, Germany*

[d]*Laboratório de Materiais Inorgânicos, Departamento de Química, Centro de Ciências Naturais e Exatas, Universidade Federal de Santa Maria, 97105-900 Santa Maria-RS, Brazil*

2-(2-Furyl)-3-hydroxychromone (HL) reacts with M^{II} ions in the formation of quadratic $[Cu(L)_2]$ (**3**), octahedral $[M(L)_2(OH_2)_2]$ (M = Co (**1**), Ni (**2**), Zn (**4**), Mn (**5**)) and seesaw $[M(L)_2]$ (M = Sn (**6**), Pb (**7**)) complexes. Recrystallization of complexes **1**-**3** in presence of pyridine lead to $[M(L)_2(py)_2]$ (**1a**-**3a**) adducts. All compounds were characterized by Fourier transform infrared spectroscopy (FTIR). Complexes **1**-**7** were analyzed by UV-Vis and diffuse reflectance spectroscopies. The estimated band gap energies range from 2.90-3.15 eV. The crystal structure of complexes **6** and **7** revealed the influence of the stereochemically active lone pair due to their electronic configuration ns^2. An intense fluorescence emission band centered at approximately 600 nm (λ_{exc} centered at 340 nm) has been observed for complex **6** in the solid state. In *N*,*N*-dimethylformamide (DMF) solution, complex **6** showed two emission bands (468 and 538 nm) when excited from 300 to 380 nm, and only one emission band (468 nm) when excited from 385 to 420 nm.

Keywords: chromone, fluorescence, molecular structure, coordination compounds

Introduction

Chromones comprehend an important class of naturally occurring compounds whose carbon skeleton exist in wide range of structural diversity.[1] Chemical and biological aspects of chromones (also known as 4*H*-chromen-4-ones) have been studied in detail because of their usefulness as biologically active agents. Some pharmacological properties attributed to molecules containing the chromone skeleton include antifungal, antiallergenic, antiviral, antihypertensive, antioxidant and anticancer activities.[2,3] Important chromone derivatives are flavone, flavonol and isoflavone (Figure 1).[4]

Flavonoids are the 2-phenyl chromone derivatives. They are found in fruits, vegetables, grains, bark, roots, stems, flowers, tea and wine. Flavonols represent a specific class of flavonoids, and are widely present in leaves, flowers and fruits as glucosides.[5] In flavonols a hydroxy group is present (Figure 1) being so-called as 3-hydroxyflavone (3HF). However, different substituents can be present in the 2-position of the chromone skeleton, such as a furyl group (Figure 2). We will represent the resulting 3-hydroxychromone-furyl-substituted molecule as 3HC-F (an alternatively as HL when its deprotonation is intended to be noted). An electron donating furyl group will affect the chemical and pharmacological properties of the molecule when compared with 3HF. Special attention arouses also for studies of its interaction with metal ions.

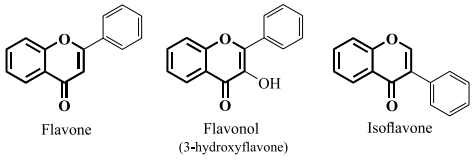

Figure 1. Chemical structure of flavone, flavonol and isoflavone. The chromone skeletal is highlighted.

*e-mail: vaniaschwade@gmail.com

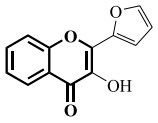

Figure 2. Chemical structure of 2-(2-furyl)-3-hydroxychromone, the HL ligand of this work.

The spectroscopic properties of 3-hydroxyflavones (3HFs) allowed their application as prospective sensors of polarity, ions and electric fields, as well as probes to study polymers, reverse micelles, lipid membranes and proteins.[6] Their strong electron conjugation provides them fluorescent property, which make them used as imaging agents for therapeutic purpose.[7] It is well known that 3HF undergoes excited-state intramolecular proton transfer (ESIPT). Dual fluorescence emission can be observed: the normal form of the excited state (N*) and the excited-state tautomeric form (T*), which emit in the blue and green, respectively. The dynamics of the ESIPT and BPT (ground-state back proton transfer) processes in 3HF using Shpol'skii spectroscopy has been performed and compared with 2-(2-furyl)-3-hydroxychromone (3HC-F). The furyl substituent has shown a strong influence on the proton tunneling rates in *n*-octane.[8] Studies on the steric effects on the fluorescence quantum yields of substituted 3-hydroxychromones (3HCs) have shown that the furan- and benzofuran-substituted 3HCs are advantageous with respect to 3HFs for the development of prospective fluorescence probes.[9] Antioxidant activity of 3HC-F and their derivatives has been evaluated using 2,2-diphenyl-1-picrylhydrazyl (DPPH). The DPPH radical reacts with electron donating molecules (antioxidants).[10]

Chelates can be formed by interactions of 3HFs with metal ions. It can be crucial in the prevention of free radical generation, which damage target biomolecules, protecting them against oxidative stress. Metal complexes have been more effective in free radicals scavenging than the free flavonoids.[11,12] A furan substituent in the 2-position of the chromone may affect the acidity of the 3-hydroxy group and the bond order of the 4-carbonyl group and, therefore, the basicity of its oxygen atom.[8] According to our knowledge, there is only one reported 2-(2-furyl)-3-hydroxychromone metallic complex, which has the suggested formula $[VO(L)_2]$.[13]

In order to contribute with the coordination chemistry of 3HC-F, the present work presents the obtention of M^{II} complexes with 2-(2-furyl)-3-hydroxychromone (3HC-F) acting as ligand (Figure 2). The Mn^{II}, Co^{II}, Ni^{II}, Cu^{II}, Zn^{II}, Sn^{II} and Pb^{II} complexes were characterized by spectroscopic techniques and elemental analysis. The complexes have formula $[M(L)_2(OH_2)_2]$ (M = Co, Ni, Zn and Mn) and $[M(L)_2]$ (M = Cu, Sn, Pb). Fluorescent properties were evaluated for the Sn^{II} complex. Complexes $[M(L)_2(py)_2]$ (M = Co, Ni and Cu) were also formed in recrystallization processes using mixtures with pyridine. X-ray diffractometry was used for analysis of the molecular structures of the ligand (a new polymorph) and six complexes.

Experimental

Chemicals and apparatus

Chemicals 2'-hydroxyacetophenone and furan-2-carboxaldehyde (Sigma-Aldrich, Saint Louis, USA) were used without purification for preparation of the corresponding furyl-substituted chalcone. Solvents ethanol (Dinâmica, Indaiatuba, Brazil) and methanol (Vetec, Rio de Janeiro, Brazil) were used as received. The metal salts for the synthesis of the complexes were obtained from commercial sources (Sigma-Aldrich, Saint Louis, USA and Dinâmica, Indaiatuba, Brazil). The elemental analyses were performed on a PerkinElmer 2400 series II. UV-Vis spectra in *N*,*N*-dimethylformamide were collected on a Shimadzu UV-2600 spectrophotometer. Solid state UV-Vis and diffuse reflectance spectra were obtained on a Shimadzu UV-2600 spectrophotometer equipped with an integrating sphere ISR 2600 Plus (barium sulfate plate was used as white reference material). Fourier transform infrared (FTIR) spectra (attenuated total reflectance (ATR) mode) were recorded on a Bruker Vertex 70 spectrophotometer in the 4000-200 cm^{-1} range (4 cm^{-1} of resolution). Electrospray ionization (ESI) high-resolution mass spectrometry (HRMS) was used for acquisition of mass spectra for the ligand on an Agilent 6210 spectrometer (positive mode) in methanol. Nuclear magnetic resonance (NMR) spectra were recorded on a Bruker BioSpin GmbH spectrometer, operating at 600 MHz for ^1H nuclei, using $CDCl_3$ or dimethyl sulfoxide (DMSO-d_6) as solvent. Solid state fluorescence excitation/emission maps were obtained in a Varian Cary Eclipse fluorimeter operating at 3D mode, monitoring the emission intensity from 390 to 750 nm (solid state) and 300 to 700 nm (*N*,*N*-dimethylformamide solutions, 3×10^{-5} mol L^{-1}), both with excitation wavelength between 280 and 420 nm (slit of 5 nm). Antistatic gloves were used in some manipulations with the samples.

Powder X-ray diffraction data of 2-(2-furyl)-3-hydroxychromone (HL) was obtained in a Bruker D8 Advance diffractometer (Cu $K\alpha_1$ λ 1.5406 Å) from 5 to 60º in a 2θ angle, using slit of 0.2º, 0.5 s *per* step and step size of 0.01º. The single crystal X-ray diffraction data collection were performed on a Bruker D8 Venture Photon 100 diffractometer with graphite monochromated Ag Kα

radiation (λ 0.56086 Å) (Pb^{II} complex) or Mo Kα radiation (λ 0.71073 Å) (Cu^{II} and Zn^{II} complex). The single crystal data collection for the chromone ligand and the Co^{II}, Ni^{II} and Sn^{II} complexes were performed on a Bruker D8 Quest diffractometer with Cu Kα radiation (λ 1.54178 Å). The structures were solved by Intrinsic Phasing method, and least-squares refinement of the structures was performed by the SHELXL-2018 program.[14] All the non-hydrogen atoms were refined anisotropically. The hydrogen atoms were placed in calculated positions and refined isotropically. Data collection and structure refinement parameters and crystallographic data for HL and complexes **1a**, **2a**, **3a**, **4**, **6** and **7** are given in Table 1. Anisotropic thermal ellipsoid plots can be found in the Supplementary Information (SI) section (Figures S1 to S7).

Synthesis

The 2-(2-furyl)-3-hydroxychromone ligand (HL) was prepared by condensation reaction of 2'-hydroxyacetophenone with furan-2-carboxaldehyde in presence of sodium hydroxide. The chalcone thus obtained was subjected to reaction conditions with hydrogen peroxide, according to the literature.[15,16]

HL

Yellow solid; yield: 65%; ^{1}H NMR (600.1 MHz, $CDCl_3$) δ 6.65 (dd, 1H, *J* 3.5, 1.7 Hz), 7.35 (d, 1H, *J* 3.5 Hz), 7.40 (t, 1H, *J* 7.5 Hz), 7.60 (d, 1H, *J* 8.5 Hz), 7.73-7.64 (m, 2H), 8.24 (dd, 1H, *J* 8.0, 1.5 Hz); ^{13}C NMR (150.9 MHz, $CDCl_3$) δ 112.8, 115.7, 118.5, 121.5, 124.7, 125.6, 133.6, 136.8, 139.1, 144.7, 144.8, 155.3, 172.7; HRMS (ESI) *m/z*, calcd. for $C_{13}H_9O_4$ $[M + H]^+$: 229.0501, found: 229.0489; calcd. for $C_{13}H_8O_4Na$ $[M + Na]^+$: 251.0320, found: 251.0315; calcd. for $C_{26}H_{16}O_8Na$ $[M_2 + Na]^+$: 479.0743, found: 479.0723.

Synthesis of the metal complexes

The HL ligand (91 mg, 0.40 mmol) was dissolved in 15 mL of methanol under mild heating (60 ºC). Then, the corresponding metal acetate (0.20 mmol), dissolved in 3 mL of methanol, was added. Immediately, a precipitate started to be formed. After 1 h of stirring at 60 ºC, the solid

Table 1. Crystal structure and refinement data for HL and complexes **1a**, **2a**, **3a**, **4**, **6** and **7**

Compound	HL	$[Co(L)_2(py)_2]$ (**1a**)	$[Ni(L)_2(py)_2]$ (**2a**)	$[Cu(L)_2(py)_2]$ (**3a**)	$[Zn(L)_2(OH_2)_2]\cdot½H_2O$ (**4**)	$[Sn(L)_2]$ (**6**)	$[Pb(L)_2]$ (**7**)
Molecular formula	$C_{13}H_8O_4$	$C_{36}H_{24}CoN_2O_8$	$C_{36}H_{24}NiN_2O_8$	$C_{36}H_{24}CuN_2O_8$	$C_{26}H_{19}O_{10.50}Zn$	$C_{26}H_{14}O_8Sn$	$C_{26}H_{14}O_8Pb$
Formula weight / (g mol^{-1})	228.19	671.50	671.28	676.11	564.78	573.06	661.56
Temperature / K	296(2)	296(2)	296(2)	297(2)	100(2)	296(2)	299(2)
Wavelength / Å	1.54178	1.54178	1.54178	0.71073	0.71073	1.54178	0.56086
Crystal system	monoclinic	monoclinic	monoclinic	monoclinic	monoclinic	monoclinic	monoclinic
Space group	$P2_1$	$P2_1/n$	$P2_1/n$	$P2_1/n$	$C2/c$	$C2/c$	$C2/c$
a / Å	10.1036(14)	13.990(3)	13.987(4)	13.887(5)	31.064(6)	21.165(6)	21.290(9)
b / Å	4.7456(9)	6.2959(14)	6.314(2)	6.2964(8)	4.7468(9)	4.9405(10)	4.752(3)
c / Å	11.0464(19)	17.355(3)	17.206(5)	17.431(5)	15.627(3)	21.139(4)	21.849(12)
α / degree	90	90	90	90	90	90	90
β / degree	103.766(15)	99.154(9)	98.60(3)	101.078(15)	110.35(3)	93.376(10)	94.59(2)
γ / degree	90	90	90	90	90	90	90
Volume / Å^3	514.43(15)	1509.2(5)	1502.6(8)	1495.7(7)	2160.4(8)	2206.6(8)	2203.1(19)
Z	2	2	2	2	4	4	4
Absorption coefficient / mm^{-1}	0.929	4.960	1.436	0.790	1.206	9.676	4.221
F(000)	236	690	692	694	1156	1136	1264
Reflections collected/ independent	8160/1824 [R(int) = 0.0305]	27218/2980 [R(int) = 0.0553]	9345/2936 [R(int) = 0.0622]	39970/4553 [R(int) = 0.0364]	15490/2367 [R(int) = 0.0280]	9525/2153 [R(int) = 0.0362]	17222/2724 [R(int) = 0.0608]
Data/restraints/ parameters	1824/1/157	2980/0/214	2936/0/214	4553/0/214	2367/3/183	2153/0/159	2724/0/159
Goodness-of-fit on F^2	1.090	1.039	1.032	1.042	1.062	1.094	1.031
Final R indices [I > 2sigma(I)]	R1 = 0.0309, wR2 = 0.0733	R1 = 0.0364, wR2 = 0.0882	R1 = 0.0557, wR2 = 0.1258	R1 = 0.0344, wR2 = 0.0940	R1 = 0.0229, wR2 = 0.0578	R1 = 0.0274, wR2 = 0.0659	R1 = 0.0297, wR2 = 0.0457
R indices (all data)	R1 = 0.0371, wR2 = 0.0771	R1 = 0.0444, wR2 = 0.0938	R1 = 0.0989, wR2 = 0.1487	R1 = 0.0533, wR2 = 0.1034	R1 = 0.0255, wR2 = 0.0593	R1 = 0.0304, wR2 = 0.0682	R1 = 0.0477, wR2 = 0.0497
Largest diff. peak and hole / (e Å^{-3})	0.126 and –0.108	0.169 and –0.317	0.232 and –0.461	0.269 and –0.463	0.396 and –0.353	0.482 and –0.418	1.166 and –0.690

a-*c* and α-γ: unit cell parameters; Z: formula unit *per* unit cell; F(000): structure factor in the zeroth-order case h = k = l = 0; F^2: squared structure factor; R1 and wR2: R-factor and weighted R-factor, respectively (both values are given by considering only the intensities I > 2σ(I)).

was isolated by simple filtration, washed with methanol and dried.

$[Co(L)_2(OH_2)_2]\cdot ½H_2O$ (**1**)

Brown solid; yield: 87 mg (79%); anal. calcd. for $C_{26}H_{19}O_{10.5}Co$ (558.36 g mol^{-1}): C 55.93, H 3.43%, found: C 55.95, H 3.29%.

$[Ni(L)_2(OH_2)_2]$ (**2**)

Orange solid; yield: 80 mg (73%); anal. calcd. for $C_{26}H_{18}O_{10}Ni$ (549.11 g mol^{-1}): C 56.87, H 3.30%, found: C 56.33, H 3.32%.

$[Cu(L)_2]$ (**3**)

Green solid; yield: 86 mg (83%); anal. calcd. for $C_{26}H_{14}O_8Cu$ (517.93 g mol^{-1}): C 60.29; H 2.72%, found: C 59.77; H 2.70%.

$[Zn(L)_2(OH_2)_2]\cdot ½H_2O$ (**4**)

Yellow solid; yield: 67 mg (60%); anal. calcd. for $C_{26}H_{19}O_{10.5}Zn$ (564.81 g mol^{-1}): C 55.29, H 3.39%, found: C 54.95, H 3.27%; ^{1}H NMR (600.1 MHz, DMSO-d_6) δ 6.78 (s, 1H), 7.46 (t, 1H, *J* 6.0 Hz), 7.61 (d, 1H, *J* 2.0 Hz), 7.84-7.69 (m, 2H), 7.96 (s, 1H), 8.18 (d, 1H, *J* 7.9 Hz).

Yellow crystals of complex **4** were obtained by dissolution of the solid in *N*,*N*-dimethylformamide and analyzed by single crystal X-ray diffraction.

$[Mn(L)_2(OH_2)_2]\cdot H_2O$ (**5**)

Yellow solid; yield: 69 mg (63%); anal. calcd. for $C_{26}H_{20}O_{11}Mn$ (563.37 g mol^{-1}): C 55.43, H 3.58%, found: C 55.88, H 3.24%.

Greenish-yellow crystals of complex **5** were obtained in a methanol/pyridine solution which were analyzed by single crystal X-ray diffraction. However, the crystals lose the crystallinity in all attempts of measurements at room temperature, not allowing the completeness of the data.

$[Sn(L)_2]$ (**6**)

$SnCl_2\cdot 2H_2O$ (45 mg, 0.20 mmol) was used; yellow solid; yield: 86 mg (75%); anal. calcd. for $C_{26}H_{14}O_8Sn$ (573.09 g mol^{-1}): C 54.49, H 2.46%, found: C 54.15, H 2.37%.

Yellow crystals of complex **6** were obtained in the methanolic mother solution and analyzed by single crystal X-ray diffraction.

$[Pb(L)_2]$ (**7**)

Yellow solid; yield: 108 mg (82%); anal. calcd. for $C_{26}H_{14}O_8Pb$ (661.58 g mol^{-1}): C 47.20, H 2.13%, found: C 46.55, H 1.80%.

Yellow crystals of complex **7** were obtained by dissolution in a pyridine/methanol mixture and analyzed by single crystal X-ray diffraction.

$[M(L)_2(py)_2]$ (M = Co (**1a**); Ni (**2a**); Cu (**3a**))

Complexes **1-3** were dissolved in a pyridine/methanol or pyridine/dimethyl sulfoxide mixture and stirred for about 10 min. After few days, rectangular yellow to orange crystals of complexes **1a-3a** were observed and collected for analysis. Complexes **1a**-**3a** were suitable for single crystal X-ray diffraction analysis.

Results and Discussion

Synthesis and structural analysis

The preparation of the 2-(2-furyl)-3-hydroxychromone molecule followed the literature,[15,16] in a two-step synthesis: (*i*) preparation of the chalcone; (*ii*) preparation of the corresponding chromone. An overview about the already published nonconsensual reaction mechanisms for the formation of 2-aryl-3-hydroxychromones from the chalcone can be found in the SI section.

The HL ligand reacts with the first row transition M^{II} metals giving complexes with ML_2 composition (Scheme 1). Complexes with Co^{II} (**1**), Ni^{II} (**2**), Zn^{II} (**4**) and Mn^{II} (**5**) are suggested to have two coordinated water molecules, leading the metal centers in the complexes to an octahedral MO_6 environment. The Cu^{II} complex (**3**) has probably a quadratic CuO_4 geometry. Complexes **6** (Sn^{II}) and **7** (Pb^{II}) shall present the effect of the ns^2 lone pair of electrons in the coordination geometry, leading to hemidirected structures. This type of structure energetically minimizes, for example, antibonding Pb^{II} np (6s-np) interactions.[17] The absence of coordinated water molecules in complexes **3**, **6** and **7** was confirmed by the FTIR spectra. On the other hand, O–H stretching and bending vibrations bands were observed in the spectra of complexes **1**, **2**, **4** and **5**.

In a tentative reaction of HL with zinc(II) chloride without heating or addition of base, yellow crystals of a new polymorph of HL were formed in the mother solution. An alternate packing of the compound lead to a distinct unit cell identification. In our case, HL crystallized in the monoclinic crystal system with formula unit *per* unit cell (*Z*) = 2. The molecule was solved in $P2_1$ space group. A close analysis of the packing and hydrogen bonds in the solid state differs from the greenish-yellow polymorph described by Wera *et al.*[18] in which the inversely oriented molecules form dimers through a pair of O–H···O interactions. The C–O and C–C bond lengths in the 3-hydroxy-4-pyrone fragment are similar in both polymorphs (Table 2).

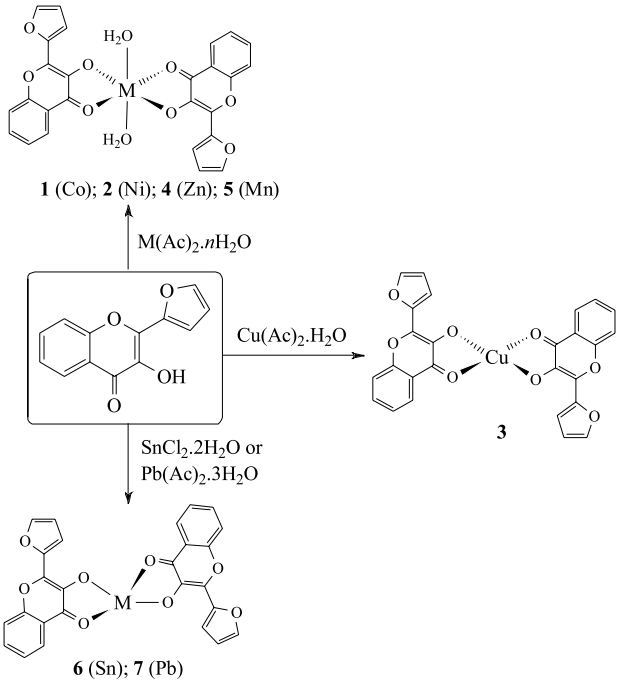

Scheme 1. Synthesis of 2:2 M^{II} complexes. Conditions: methanol, 1 h, 60 ºC.

Table 2. Selected bond lengths in HL in comparison with the previous related polymorph

Bond	This work / Å	Literature[18] / Å
C(1)–O(1)	1.353(3)	1.3503(19)
C(2)–O(2)	1.241(2)	1.2419(19)
C(1)–C(2)	1.436(3)	1.443(2)
C(1)–C(9)	1.356(3)	1.364(2)
C(2)–C(3)	1.450(3)	1.464(2)

The yellow HL polymorph of this work shows inter- and intramolecular O–H···O hydrogen bonds interactions in the solid state (Figure 3 and Table 3). The molecules are associated by hydrogen bonds and π-stacking interactions in the [0 1 0] crystallographic direction. The π-stacking arrangement occurs between the aromatic C3–C8 ring and the pyrone ring (which contains the O4 atom). The centroid-centroid distance is 3.5842(16) Å.

In the FTIR spectrum of HL, the O–H stretching vibration band appeared at 3243 cm^{-1}. The band at 1610 cm^{-1} is assigned to the C=O (main contribution) and C=C stretching vibrations.[19] Comparisons of some vibration modes of HL with those found in the coordination compounds will be presented further in the text.

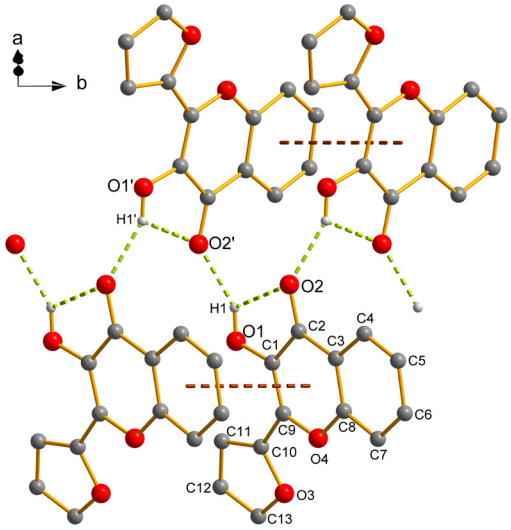

Figure 3. Solid state arrangement of HL (yellow polymorph). Aromatic hydrogen atoms were omitted for clarity. Symmetry code: ' $-x + 2$, $y - 1/2$, $-z + 2$.

The reaction of zinc(II) acetate with HL in methanol under heating yielded complex $[Zn(L)_2(OH_2)_2]\cdot½H_2O$ (**4**). Yellow rectangular block shaped crystals were obtained in the mother solution or in recrystallization process using *N*,*N*-dimethylformamide. The monoanionic chromonate ligands coordinate in the equatorial positions being the axial positions occupied by water molecules (Figure 4). The coordinated water molecules establish intermolecular O–H···O hydrogen bonds (Table 3) with neighboring molecules. They are reinforced by π-stacking interactions (centroid-centroid distances of 3.4077(11) Å). π-Stacking, in this complex, occurs between the furyl (which contains the O3 atom) and pyrone (which contains the O4 atom) rings.

Table 3. Hydrogen bonds for HL and complex **4**

	D–H...A	d(D–H) / Å	d(H...A) / Å	d(D...A) / Å	< (DHA) / degree
HL	O(1)–H(1)...O(2)	0.88	2.30	2.742(2)	111.0
	O(1)–H(1)...O(2)'	0.88	1.93	2.701(2)	145.9
4	O(5)–H(5A)...O(1)''	0.856(15)	1.885(16)	2.7171(15)	163.9(19)
	O(5)–H(5B)...O(2)'''	0.821(15)	2.146(17)	2.8890(16)	150.5(19)
	O(6)–H(6A)...O(5)	0.791(19)	2.52(2)	3.309(3)	177(6)
	O(6)–H(6A)...O(1)	0.791(19)	2.60(5)	2.9207(13)	106(4)

Symmetry transformations used to generate equivalent atoms: ' $-x + 2$, $y - 1/2$, $-z + 2$; '' x, $y - 1$, z; ''' $-x$, $-y - 1$, $-z$.

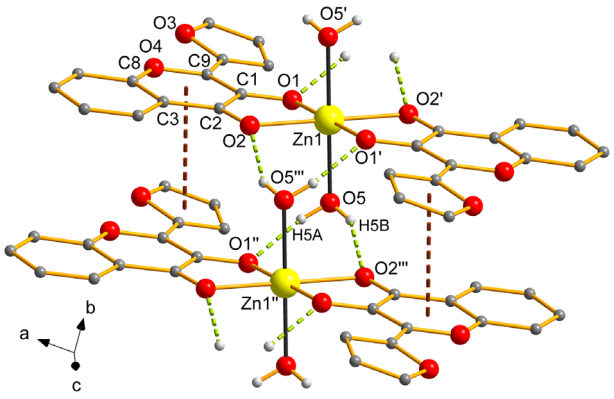

Figure 4. Solid state interactions of complex **4**. Aromatic hydrogen atoms and solvate water molecule were omitted for clarity. Symmetry codes: ' $-x, -y, -z$; '' $x, y-1, z$; ''' $-x, -y-1, -z$.

The $Zn–O_{(chromonate)}$ bond lengths are 2.05 and 2.10 Å. For comparison, these distances are between those found in the Zn^{II} mixed complex $[Zn(tmen)(L)_2]$ (tmen = *N*,*N*,*N*',*N*'-tetramethylethylenediamine; HL = 3-hydroxyflavone) (1.98 and 2.24 Å).[20] The coordination of the carbonyl oxygen O2 caused a shift of the ν(C=O) band in the FTIR spectrum, from 1610 to 1547 cm^{-1}. Similar shift has been observed for d^{10} complexes with 3-hydroxyflavone.[20] The $Zn–O_{(water)}$ bond lengths are 2.17 Å. In the IR spectrum, the O–H vibrations were observed at 3505 and 1677 cm^{-1}.

The reactions of Sn^{II} and Pb^{II} salts lead to formation of isostructural $[M(L)_2]$ complexes. Figure 5 shows the pseudo-polymeric structure of the Sn^{II} complex (**6**). No additional figure is presented for the Pb^{II} complex (**7**) since it is virtually identical to the Sn^{II} complex. In both complexes the lone pair is stereochemically active, leading to M···O interactions in the solid state. The Sn···O and Pb···O distances are 3.809(2) and 3.543(4) Å, respectively. These distances are within the sum of the van der Waals radii of the corresponding atoms.[21] The intermolecular M···O interactions produces pseudo-polymeric arrangements in the [0 1 0] crystallographic direction.

Complex **6** represents the first structurally characterized Sn^{II}-chromone complex. We could find only one Sn^{IV} complex with 3-hydroxyflavone (HL). In the $[Ph_2Sn^{IV}Cl(L)]$ complex, the Sn–O bond lengths are 2.06 and 2.24 Å.[22] In complex **6**, the Sn–O bond lengths are 2.1210(18) and 2.373(2) Å (Table 4). The Pb–O bond lengths in complex **7** are 2.250(3) and 2.481(3) Å, which are close to the distances found in a mixed Pb^{II} complex with 3-hydroxyflavone (2.23 and 2.60 Å). This six-coordinated Pb^{II} complex has also shown hemidirected geometry (in which there is an open site in the coordination sphere).[17] There are no chromone-containing Sn^{II} complexes structurally characterized for comparison of the hemidirected coordination geometry.

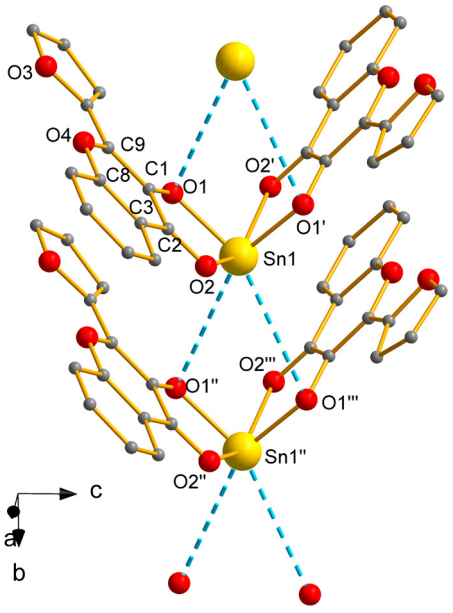

Figure 5. Solid state interactions of complex **6**. Aromatic hydrogen atoms were omitted for clarity. Symmetry codes: ' $-x+1, y, -z+3/2$; '' $x, y+1, z$; ''' $-x+1, y+1, -z+3/2$.

Complexes **1**-**3** were soluble in pyridine. Crystals were obtained in solvent mixtures with pyridine, such as MeOH/py and DMSO/py. Octahedral $[M(L)_2(py)_2]$ (**1a**-**3a**) complexes were formed (Scheme 2). Ligand substitution reactions are suggested for complexes **1a** and **2a** formation. Water molecules are replaced by pyridine molecules in the axial positions. In case of complex **3a** formation, pyridine molecules probably coordinate in axial positions of the quadratic complex **3**.

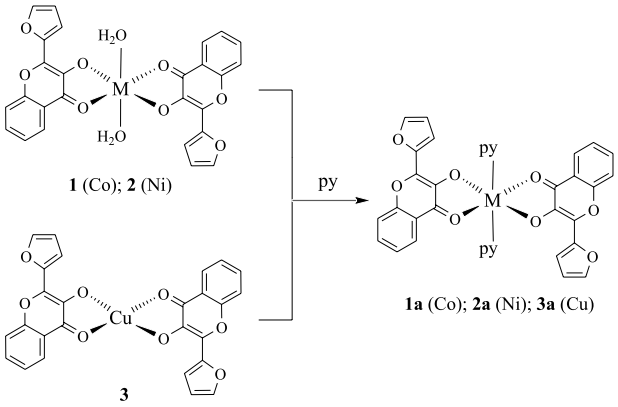

Scheme 2. Preparation of the pyridine adducts **1a**, **2a** and **3a**.

Complex **5** was also soluble in pyridine, and crystals in MeOH/py were obtained. However, the crystals were not stable for enough time for collection of the full X-ray diffraction data at room temperature. The reason of it is probably the volatile methanol molecules in the crystals of complex $[Mn(L)_2(OH_2)_2]$·MeOH. It is remarkable that,

in this case, the ligand substitution did not occur. Thus, all the observations with complexes **1**, **2**, **3** and **5** led us to conclude that the Mn^{II} ion, as a harder Lewis acid when compared with Co^{II} and Cu^{II} ions, prefers the coordination with water (a hard base) rather than the coordination of pyridine (a soft base when compared with water).

The structural analysis by single crystal X-ray diffraction could be realized for complexes **1a**-**3a**. These isostructural *trans*-$[M(L)_2(py)_2]$ complexes are structurally similar to 3-hydroxyflavone complexes with Ni^{II},[23] Cu^{II} [24] and Mn^{II}.[25] By analysis of the crystal packing, intermolecular π-stacking interactions between the furyl group and the chromone rings of the adjacent molecule can be found. In complex **1a**, the centroid-centroid distances are 3.6532(16) and 3.7074(15) Å. Figure 6 presents one of the π-stacking possibilities (furyl group containing O3 atom and the C3–C8 ring) for complex **1a**.

The M–O bond lengths of 1.95-2.35 Å (Table 4) in complexes **1a**-**3a** are between those reported for Ni^{II}, Cu^{II} and Mn^{II} complexes with 3-hydroxyflavone.[23-25] The M–N(py) bond lengths of 2.07-2.18 Å are between the distances of the mentioned complexes (1.93-2.18 Å). Bond angles O(1)–M(1)–O(1)', O(2)–M(1)–O(2)' and N(1)–M(1)–N(1)' (symmetry code: '$-x + 1, -y + 1, -z + 1$) are 180º. A detailed table with bond angles for the complexes can be found in Table S1 (SI section).

FTIR and UV-Vis characterization

The most prominent feature in the FTIR spectra of the complexes, compared to the spectra of the HL ligand, is the absence of the O–H stretching vibration band at around 3200 cm^{-1}. In the spectra of complexes **1**, **2**, **4** and **5** the band at 3400-3500 cm^{-1} is due to the O–H stretching vibration of the coordinated water molecules. The weak and well-defined bands at around 1680 cm^{-1} in these spectra are attributed to the water O–H bending vibration. A significant shift of the C=O stretching vibration band to lower wavenumbers has been observed in the complexes, from 1610 to ca. 1545 cm^{-1}. Additionally, the bands at

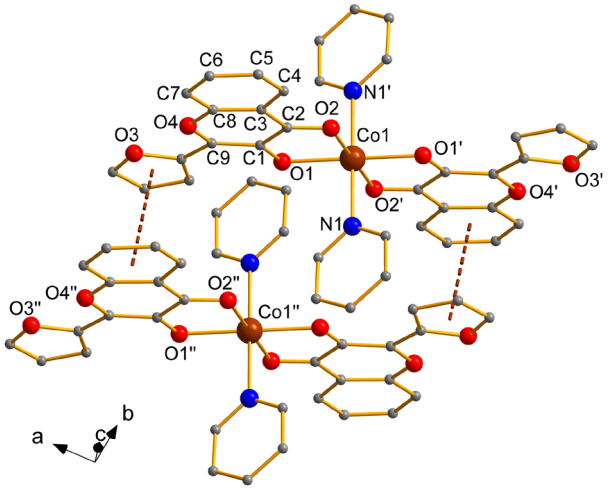

Figure 6. Solid state interactions of complex **1a**. Hydrogen atoms were omitted for clarity. Symmetry codes: ' $-x + 1, -y + 1, -z + 1$; " $x, y - 1, z$.

1347-1356 cm^{-1}, related to ν(C–O) vibration, shifted to higher wavenumbers in the spectra of the complexes when compared to the free ligand (1328 cm^{-1}). These shifts arise as a result of the formation of a five-membered ring with the chelation of $[L]^-$ to the metal centres.[22,25-27] The presence of pyridine in complexes **1a**, **2a** and **3a** could be evidenced by the medium intensity band at around 700 cm^{-1} (δ(C–H)). The relevant FTIR spectral data are compiled in Table 5. The spectra can be found in Figures S13 to S23 (SI section). Information about calculated vibrations of the chromone skeletal have been described in the literature.[19,28]

Electronic UV-Vis characterization was performed in the solid state and in solution for HL and complexes **1**-**7**. In the solid state HL spectrum, broad bands centered at approximately 250, 315 and 390 nm were observed (Figure 7). Additionally, there is a shoulder at around 455 nm. For comparison, in solution (cyclohexane, acetonitrile and methanol), two sets of main bands were described: from 270 to 370 nm (set I) and around 250 nm (set II).[15]

In the HL molecule, there are four oxygen atoms which have non-bonding electrons. Among these, oxygen belonging to furan ring show absorption band in the higher

Table 4. Selected bond lengths in complexes **1a**, **2a**, **3a**, **4**, **6** and **7**

Bond	**1a** (M = Co) / Å	**2a** (M = Ni) / Å	**3a** (M = Cu) / Å	**4** (M = Zn) / Å	**6** (M = Sn) / Å	**7** (M = Pb) / Å
M(1)–O(1)	2.0210(12)	2.028(2)	1.9498(11)	2.0530(12)	2.1210(18)	2.250(3)
M(1)–O(2)	2.1568(14)	2.091(2)	2.3544(13)	2.1043(11)	2.373(2)	2.481(3)
M(1)–O(5)	–	–	–	2.1699(11)	–	–
M(1)–N(1)	2.1818(17)	2.122(3)	2.0700(15)	–	–	–
C(1)–O(1)	1.308(2)	1.309(4)	1.3068(18)	1.3146(17)	1.321(3)	1.319(4)
C(2)–O(2)	1.253(2)	1.255(4)	1.2417(18)	1.2628(18)	1.241(3)	1.257(5)
C(1)–C(2)	1.446(3)	1.438(5)	1.459(2)	1.4437(19)	1.431(4)	1.428(5)

Table 5. Selected FTIR spectral data of HL and the metal complexes

Compound	Band / cm^{-1}								
	ν(O–H)	ν(C–H)	δ(O–H)	ν(C=O)	ν(C=C) + δ(C–H)	ν(C–O(H))	ν(C–O–C)	δ(C–C)	δ(C–H)$_{py}$
HL	3243	3158-3061	–	1610	1488, 1421	1328	1269	757, 738	–
1	3499	3139-3039	1684	1546	1487, 1415	1355	1259	754, 742	–
1a	–	3147-3061	–	1552	1492, 1439, 1414	1347	1261	743	701
2	3395	3141-3054	1687	1547	1487, 1418	1356	1263	752, 730	–
2a	3420	3148-3062	–	1546	1492, 1441, 1417	1349	1263	743	701
3	–	3131-3054	–	1541	1481, 1423	1350	1270	752, 729	–
3a	–	3144-3057	–	1541	1493, 1441, 1421	1348	1263	751	699
4	3505	3140-3066	1677	1547	1487, 1415	1355	1259	755, 741	–
5	3513	3140-3069	1677	1544	1487, 1414	1356	1260	754, 743	–
6	–	3141-3036	–	1547	1483, 1412	1350	1258	750	–
7	–	3147-3054	–	1541	1487, 1412	1354	1260	746	–

ν: stretching vibration; δ: bending vibration.

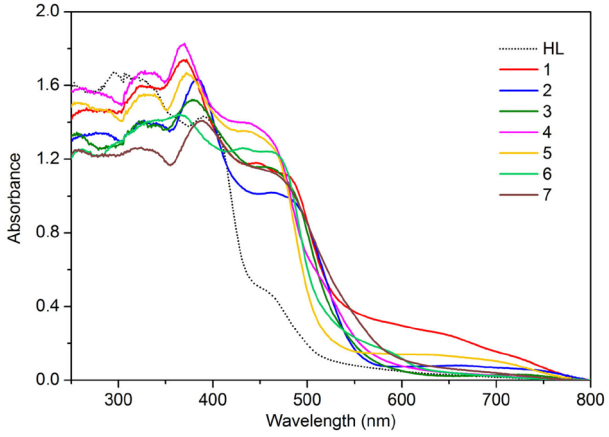

Figure 7. Solid state UV-Vis spectra of HL and its complexes **1**-**7**.

energy UV region (> 220 nm).[15] In the solid state, the broad band at 315 nm probably refers to the π-π* transition while the band at 390 nm, to the n-π* transitions. The most easily available non-bonding electrons should be those of the O atom at 4-carbonyl group. The band at 250 nm can be assigned to the benzoylic moiety of the molecule, as has been observed in solution.[15] About the shoulder in the visible region of the spectrum (around 455 nm) we could not find any reference in the literature. One suggestion is an intramolecular charge transfer situation due to the conjugation of the molecule. For this reason, we decided to record the UV-Vis absorption spectrum of HL in *N*,*N*-dimethylformamide solution (Figure S12, SI section). We could identify a clear weak absorption band centered at around 430 nm. It suggests that the band at 455 nm does not refers to a specific effect in the solid state.

In the solid state UV-Vis spectra of complexes **1**-**7**, the π-π* transition band appears centered at ca. 327 nm. The n-π* transitions are centered in the 368-390 nm range. However, the main difference of the spectra of the complexes in comparison with the spectrum of HL are the more intense bands in the visible region, from 420 to ca. 525 nm. These bands can be assigned to charge transitions between the metal ions and the chromonate ligands.

UV-Vis absorption spectroscopy analysis in *N*,*N*-dimethylformamide solution was also performed for complexes **1**-**7**. By comparison of the UV-Vis absorption spectrum of HL with the spectra of complexes **1**, **2**, **3** and **5** (complexes with transition metal ions) (Figure 8a) it can be noted that the same set of bands from 380 to 400 nm is observed for HL and complex **3** (the Cu^{II} complex proposed with a quadratic geometry). The octahedral complexes **1**, **2** and **5** showed a different profile in this region of the spectra. In the visible region of the spectra, the bands involving charge transfer between metal ions and the chromonate ligands has been observed centered at 432-453 nm. In all spectra, the π-π* transition band appears at 270 nm.

Comparison of the UV-Vis absorption spectra of complexes **4**, **6** and **7** (complexes with d^{10} or ns^2 configuration) and the spectrum of HL in the same solvent was also performed (Figure 8b). Curiously, a similar profile in the absorption bands has been observed for HL and complex **6** (the Sn^{II} complex) from 288 to 400 nm. In the visible region of the spectra, the bands involving charge transfer between metal ions and the chromonate ligands were observed centered at 420-428 nm. It is thus remarkable that the isostructural complexes **6** and **7** in the solid state have distinct behavior when in solution.

Optical band gap estimation

Diffuse reflectance spectroscopy measurements of HL

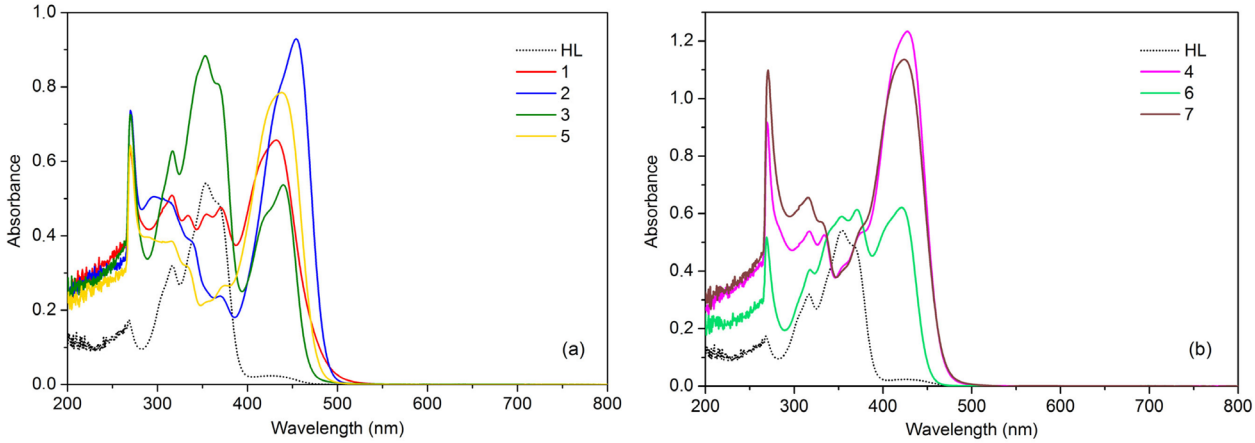

Figure 8. UV-Vis spectra of HL and complexes **1**-**7** in DMF at concentration of 3×10^{-5} mol L^{-1}.

and complexes **1**-**7** were carried out in the wavelength range of 250-800 nm. These data were treated by using the Kubelka-Munk function: $F(R) = (1 - R)^2/2R$, where R is the reflectance.[29] The Kubelka-Munk absorbance spectra can be found Figure S24 (SI section). The values of the band gap energies (E_g) were then estimated by linear extrapolation of the Tauc plots.[30] The E_g values found range from 2.90-3.15 eV (Figure 9). Optical band gap energies lower than 3.0 eV are promising for application, e.g., in photocatalysis using visible light.[31] For HL, if considered the second absorption edge which seems to be more intense, the band gap energy is 3.40 eV. In this case, all complexes present lower estimated band gap energies than HL.

Fluorescence studies

We decided to study complexes **4**, **6** and **7** by fluorescence spectroscopy. These complexes contain d^{10} ion (Zn^{II}) or $(n-1)d^{10}ns^2$ ions (Sn^{II} and Pb^{II}). Thus, these complexes would be more promising for fluorescence emission. However, preliminar analysis by solid state fluorescence showed us that the Sn^{II} complex was the candidate for further analysis. Curiously, as discussed in the UV-Vis characterization, complex **6** presented a distinct absorption profile in *N*,*N*-dimethylformamide (DMF) solution when compared with complexes **4** and **7**, specially in the 300-400 nm region. Previous report[32] described the use of fluorescent 3-hydroxyflavone (3HF) tin(IV) complexes for spectrofluorimetric determination of these species.

Measurements were performed in solid state and in DMF solution for complex **6** and HL for comparison. By analysis of the fluorescence map, in the solid state, HL presents emission bands at 420, 500 (most intense) and 530 nm when excited from approximately 290 to 350 nm (Figure 10). It is important to mention that the polymorph of HL was identified by powder X-ray diffraction (Figure S25, SI section) and corresponds to the polymorph reported by Wera *et al.*[18] These bands were also observed in the solid state fluorescence maps of complexes **4**, **6** and **7**. However, complex **6** additionally showed an intense emission band centered at approximately 600 nm. Figure S26 (SI section) shows a photograph of the complex **6** exposed to external UV-A radiation source (λ 365 nm), in which the yellow-orange fluorescence is observed. Even more intense fluorescence would be expected by using an external UV radiation source with λ 330-350 nm.

Additionally, we decided to analyze the fluorescence behavior also in solution for complex **6** and HL for comparison with the solid state behavior. In DMF solution, the HL fluorescence map presents two emission bands when excited between 280 and 382 nm (Figure 11). The weak luminescence band centered at 420 nm is attributable to the normal excited species (N*), and the intense luminescence band centered at 540 nm has been attributed to the excited tautomer (T*).[15,33] Upon excitation, N* undergoes an excited intramolecular proton transfer (ESIPT) to give T*.[33] Two emission bands were observed before in polar protic (methanol) and polar aprotic (acetonitrile) solvents, and only one band (T*) in apolar solvent (cyclohexane) with excitation wavelength of 359 nm.[15]

Complex **6** presented two emission bands (centered at 468 and 538 nm) when excited from approximately 300 to 380 nm (Figure 11). These fluorescence bands do not shift upon changing the excitation wavelength, but change their relative intensity, as observed in the color scale. It can be also observed that only one emission band (468 nm) appears when excited between 385 and 420 nm. It suggests that the band at 538 nm is related to intraligand transition emission, while the band at 468 nm is related to charge-transfer (MLCT) emission. In the literature, we could find organotin complexes with one or two emission bands in the range of

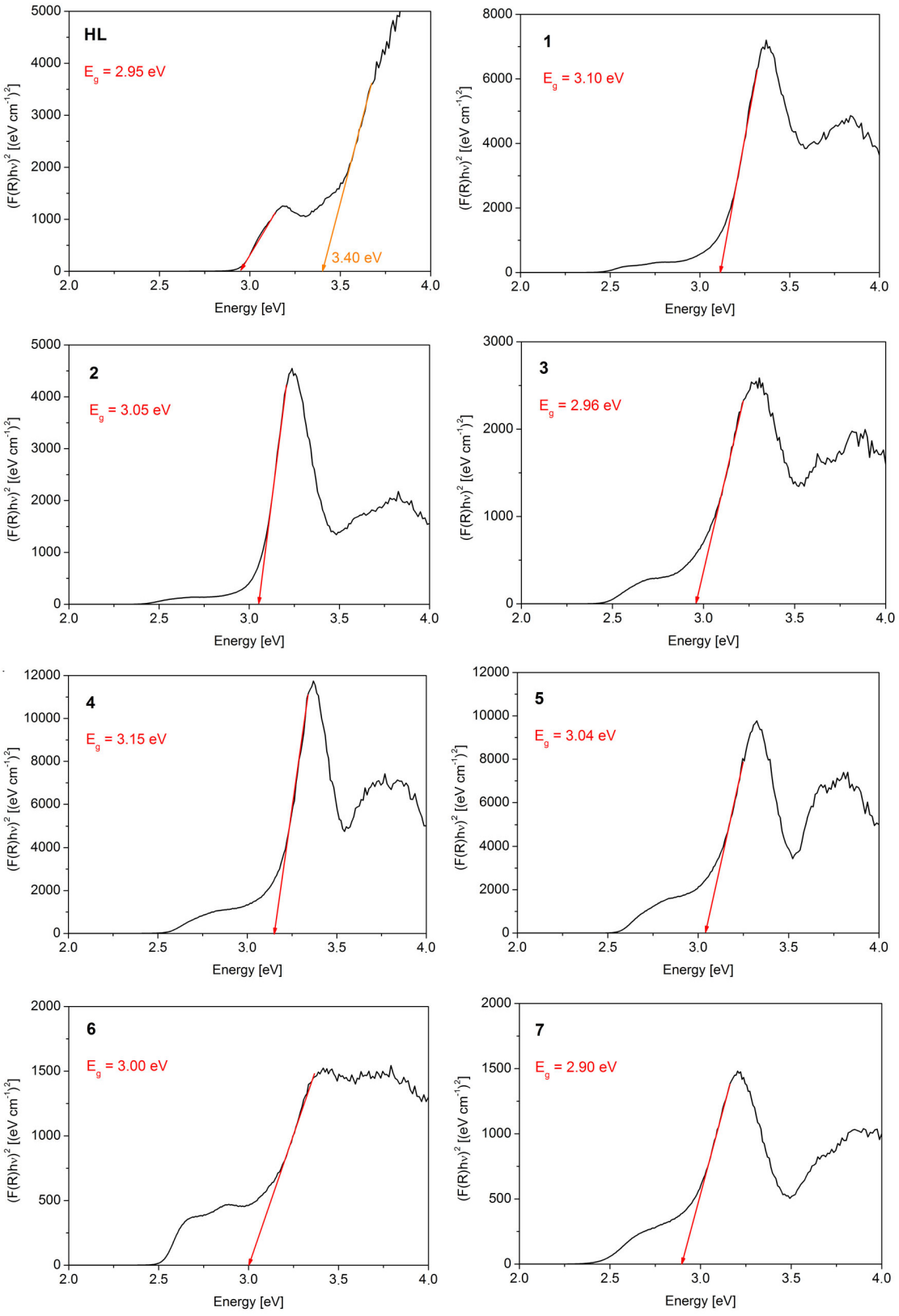

Figure 9. Optical bandgap of HL and complexes **1**-**7**.

377 to 537 nm.[34] In complex **6** the influence of the lone-pair (n) orbital of the divalent tin atom is not clear, however the literature suggests that the n-π* transition should not be near to the lowest energy π-π* transition to avoid fluorescence

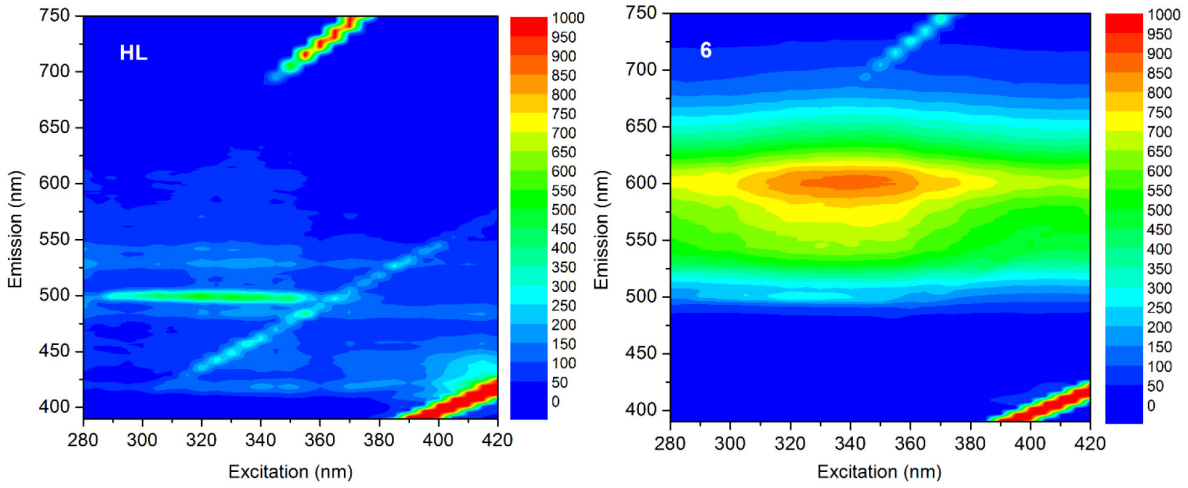

Figure 10. Fluorescence maps for HL and complex **6** in the solid state.

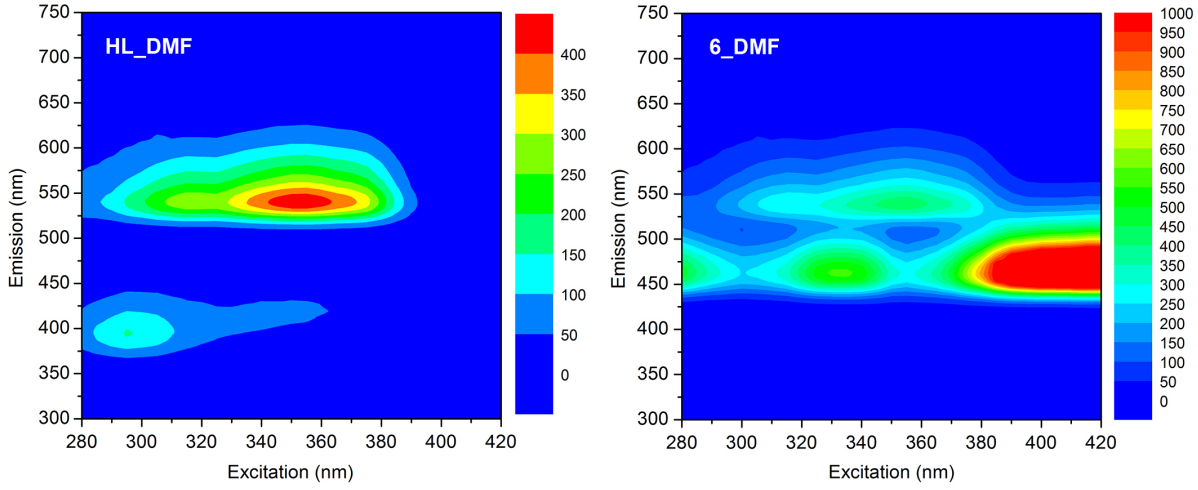

Figure 11. Fluorescence maps for HL and complex **6** in *N*,*N*-dimethylformamide solution.

quenching.[35] As observed before, solid samples show fluorescence at longer wavelengths than solution samples.[36]

Conclusions

2-(2-Furyl)-3-hydroxychromone forms stable complexes with first row transition M^{2+} ions as well as with Sn^{2+} and Pb^{2+} ions. In all complexes, within deprotonation of the ligand, coordination occurs in a chelate and *trans* form. Additional coordinated water or pyridine molecules are present in complexes $[M(L)_2(OH_2)_2]$ (M = Mn, Co, Ni, Zn) and $[M(L)_2(py)_2]$ (M = Co, Ni, Cu). Complexes with the Group 14 ions showed the active lone pair in their seesaw structures. In DMF solution, the Sn^{2+} complex presented two emission bands (468 and 538 nm) when excited under 400 nm and a single emission band (468 nm) when excited with UV and violet region wavelengths (385-420 nm). Thus, 2-(2-furyl)-3-hydroxychromone is promising as a fluorescent sensor for Sn^{2+}.

Supplementary Information

Crystallographic data (excluding structure factors) for the structures in this work were deposited in the Cambridge Crystallographic Data Centre as supplementary publication number CCDC 2046242-2046248. Copies of the data can be obtained, free of charge, via https://www.ccdc.cam.ac.uk/structures/.

Supplementary material to this article (such as thermal ellipsoid plots and spectroscopic characterization spectra of HL and complexes) is available free of charge at http://jbcs.sbq.org.br as PDF file.

Acknowledgments

This work was supported by CAPES (Coordenação de Aperfeiçoamento de Pessoal de Nível Superior-Programa de Demanda Social), process number 88882.457453/2019-01.

References

1. Panhekar, D. Y.; Satpute, S.; Deharkar, P.; Kalambe, A. B.; Renalson, K. S.; *Chem. Sci. Trans*. **2018**, *7*, 408.
2. Sharma, S. K.; Kumar, S.; Chand, K.; Kathuria, A.; Gupta, A.; Jain, R.; *Curr. Med. Chem*. **2011**, *18*, 3825.
3. Reis, J.; Gaspar, A.; Milhazes, N.; Borges, F.; *J. Med. Chem*. **2017**, *60*, 7941.
4. Ram, V. J.; Sethi, A.; Nath, M.; Pratap, R.; *The Chemistry of Heterocycles: Chemistry of Six to Eight Membered N, O, S, P and Se Heterocycles*; Elsevier Ltd.: Amsterdam/Oxford/ Cambridge, 2019.
5. Panche, A. N.; Diwan, A. D.; Chandra, S. R.; *J. Nutr. Sci*. **2016**, *5*, e47.
6. Klymchenko, A. S.; Demchenko, A. P.; *New J. Chem*. **2004**, *28*, 687.
7. Butun, B.; Topcu, G.; Ozturk, T.; *Mini-Rev. Med. Chem*. **2018**, *18*, 98.
8. Bader, A. N.; Pivovarenko, V. G.; Demchenko, A. P.; Ariese, F.; Gooijer, C.; *J. Phys. Chem. B* **2004**, *108*, 10589.
9. Bader, A. N.; Pivovarenko, V.; Demchenko, A. P.; Ariese, F.; Gooijer, C.; *Spectrochim. Acta, Part A* **2003**, *59*, 1593.
10. Kaur, R.; Kaur, K.; Bansal, M.; *Asian J. Chem*. **2016**, *28*, 1921.
11. Symonowicz, M.; Kolanek, M.; *Biotechnol. Food Sci*. **2012**, *76*, 35.
12. Grazul, M.; Budzisz, E.; *Coord. Chem. Rev*. **2009**, *253*, 2588.
13. Graphure, M.; Chaudhary, R. G.; Juneja, H.; Ingle, V.; Gandhare, N.; *J. Chin. Adv. Mater. Soc*. **2013**, *1*, 257.
14. Sheldrick, G.; *SHELXTL* version 2018/3; Program for Crystal Structure Refinement, University of Göttingen, 2018.
15. Bansal, M.; Kaur, R.; *J. Chem. Sci.* **2015**, *127*, 405.
16. Kaur, K.; Kaur, R.; Tomar, J.; Bansal, M.; *Photochem. Photobiol. Sci*. **2017**, *16*, 1311.
17. Grubel, K.; Saraf, S.; Anderson, S. N.; Laughlin, B. J.; Smith, R. C.; Arif, A. M.; Berreau, L. M.; *Inorg. Chim. Acta* **2013**, *407*, 91.
18. Wera, M.; Pivovarenko, V. G.; Sikorski, A.; Lis, T.; Blazejowski, J.; *Acta Crystallogr., Sect. E: Crystallogr. Commun.* **2011**, *E67*, o266.
19. Erdogdu, Y.; Yurdakul, S.; Badoglu, S.; Güllüoglu, M. T.; *J. Mol. Struct*. **2019**, *1184*, 364.
20. Annan, T. A.; Peppe, C.; Tuck, D. G.; *Can. J. Chem*. **1990**, *68*, 423.
21. Batsanov, S. S.; *Inorg. Mater*. **2001**, *37*, 871.
22. Villamil-Ramos, R.; Barbab, V.; Yatsimirsky, A. K.; *Analyst* **2012**, *137*, 5229.
23. Farina, Y.; Yamin, B. M.; Fun, H.-K.; Yip, B.-C.; Teoh, S.-G.; *Acta Crystallogr., Sect. C: Struct. Chem.* **1995**, *C51*, 1537.
24. Okabe, N.; Yamamoto, E.; Yasunori, M.; *Acta Crystallogr., Sect. E: Crystallogr. Commun.* **2003**, *E59*, m715.
25. Kaizer, J.; Baráth, G.; Pap, J.; Speier, G.; Giorgi, M.; Réglier, M.; *Chem. Commun*. **2007**, 5235.
26. Kahrović, E.; Zahirović, A.; Višnjevac, A.; Osmanković, I.; Turkušić, E.; Kurtagić, H.; *Croat. Chem. Acta* **2018**, *91*, 195.
27. Balogh-Hergovich, É.; Speier, G.; Argayb, G.; *J. Chem. Soc., Chem. Commun*. **1991**, 551.
28. Machado, N. F. L.; Valero, R.; Domingos, H. S.; Tomkinson, J.; Carvalho, L. A. E. B.; *Vib. Spectrosc*. **2012**, *63*, 325.
29. Nilavazhagan, S.; Anbuselvan, D.; Santhanam, A.; Chidhambaram, N.; *Appl. Phys. A* **2020**, *126*, 279.
30. Babizhetskyy, V.; Levytskyy, V.; Smetana, V.; Wilk-Kozubek, M.; Tsisar, O.; Piskach, L.; Parasyuk, O.; Mudring, A.-V.; *Z. Naturforsch*. **2020**, *75*, 135.
31. Teixeira, I. F.; Quiroz, J.; Homsi, M. S.; Camargo, P. H. C.; *J. Braz. Chem. Soc*. **2020**, *31*, 211.
32. Blunden, S. J.; Smith, P. J.; *J. Organomet. Chem*. **1982**, *226*, 157.
33. Khanna, R.; Kumar, R.; Dalal, A.; Kamboj, R. C.; *J. Fluoresc*. **2015**, *25*, 1159.
34. Jiménez-Pérez, V. M.; García-López, M. C.; Munoz-Flores, B. M.; Chan-Navarro, R.; Berrones-Reyes, J. C.; Dias, H. V. R.; Moggio, I.; Arias, E.; Serrano-Mireles, J. A.; Chaves-Reyes, A.; *J. Mater. Chem. B* **2015**, *3*, 5731.
35. Kobayashi, J.; Kushida, T.; Kawashima, T.; *J. Am. Chem. Soc*. **2009**, *131*, 10836.
36. Takano, K.; Takahashi, M.; Fukushima, T.; Takezaki, M.; Tominaga, T.; Akashi, H.; Takagi, H.; Shibahara, T.; *Bull. Chem. Soc. Jpn*. **2012**, *85*, 1210.

Submitted: December 10, 2020
Published online: April 12, 2021